Graphical and WKB analysis of nonuniform Bragg gratings

L. Poladian
Optical Fibre Technology Centre, University of Sydney, New South Wales 2006, Australia
(Received 21 July 1993)

A deeper insight into the relationship between the shape of a slowly varying nonuniform Bragg grating and its reflectance spectrum is obtained through a qualitative graphical analysis of the local photonic band gaps in the grating and a quantitative WKB (or phase-integral) approximation of the grating fields. Three different gratings—a linearly chirped grating, a moiré grating, and a Gaussian tapered grating—are analyzed in detail to illustrate the power of the technique. The results are in excellent agreement with the exact numerical results obtained via coupled-mode analysis.

PACS number(s): 42.79.Dj, 42.40.Eq

I. INTRODUCTION

Gratings in fibers or other waveguide geometries have many applications, including wavelength-selective mirrors, wavelength-selective couplers, filters, frequency references, mode converters, modulators, and pulse compressors [1–5]. The use of slowly varying gratings, where the local period or depth of modulation varies along the grating, provides extra degrees of freedom, which can be exploited in the design of grating-based devices [1,6–8]. A deeper knowledge and understanding of the relationship between the profile of the grating—that is, the variation of grating depth and/or period along the grating—and the resulting reflectance spectrum will be of benefit in grating design.

The properties of uniform gratings are well understood. If the incident field has a wavelength λ close to the Bragg wavelength of the grating it will be strongly reflected through constructive interference of the waves reflected by each period of the grating. The Bragg wavelength for a grating with average refractive index $\bar{n}$ and grating period Λ is $\lambda_B = 2\bar{n}\Lambda$. Note that the Bragg wavelength depends on both the period *and* the average refractive index. The width of the band of strongly reflected wavelengths (the "photonic band gap" or reflection band) is $\Delta\lambda = \lambda_B \Delta n/\bar{n}$, where Δn is the depth of modulation of the refractive index in the grating. When the incident wavelength lies inside the reflection band, the fields in the grating are evanescent waves (exponential functions) and most of the light is reflected. However, when the incident wavelength lies outside the reflection band, the fields in the grating are propagating waves (oscillatory functions) and most of the light is transmitted.

In a nonuniform Bragg grating, the average refractive index $\bar{n}$, the grating period λ, and the depth of modulation Δn may vary slowly along the length of the grating. At each position along the grating, the grating has a *local* Bragg wavelength and a *local* photonic band gap. When an incident wave of a given wavelength travels through the grating it will encounter two types of regions. Regions where it lies outside the *local* reflection band, interacts weakly with the grating, and will propagate without much coupling to reflected wave, and regions where it lies inside the *local* reflection band, interacts strongly with the grating, and very little light will propagate through these regions, most of it being coupled to the reflected wave.

Coupled-mode analysis and a recent effective-medium reformulation [9] of the coupled-mode equations are briefly summarized in Sec. II. In Sec. III the construction and interpretation of *reflection-band diagrams* is discussed. These diagrams display the location of the local photonic band gap as a function of position in the grating and give qualitative information about the reflectance spectrum. In Sec. IV the WKB or phase-integral method and its application to nonuniform gratings are discussed. It can be used to obtain the quantitative information about the results deduced from the reflection-band diagrams. The mathematical details of the WKB analysis are given in the Appendix. Three very different gratings have been chosen — a linearly chirped grating, a Moiré grating, and a Gaussian-tapered grating — to illustrate the techniques of Secs. III and IV. The reflection-band diagram and WKB results for each structure are analyzed in detail in Sec. V and compared to results obtained from direct solution of the coupled-mode differential equations.

II. COUPLED MODES AND EFFECTIVE-MEDIUM THEORY

The coupled-mode analysis for nonuniform gratings closely follows the standard analysis for uniform gratings [1–3]. The analysis given here is valid for gratings where the modulation depth is not too large and the variations in the depth and period of the grating are not too fast. A detailed and rigorous derivation of the coupled-mode equations using a multiple-scale analysis has been given recently [9] and can be used to include higher-order effects that become important in deeper gratings.

The refractive index variation is written as

$$n(z) = n_0 \left[1 + \sigma(z) + 2h(z)\cos\left(\frac{2\pi}{\Lambda_0} z + 2\phi(z)\right)\right], \quad (1)$$

where ϕ, σ, and h are all slowly varying quantities and describe the phase, average refractive index, and modulation amplitude of the grating, respectively, and Λ_0 is the nominal period of the Bragg grating. The detuning parameter

$$\Delta = kn_0 - \frac{\pi}{\Lambda_0} \tag{2}$$

is introduced, where k is the free-space wave number of the incident light. The electric field is written in the form

$$E(z) = u(z)\exp\left(i\frac{\pi}{\Lambda_0}z + i\phi(z)\right) + v(z)\exp\left(-i\frac{\pi}{\Lambda_0}z - i\phi(z)\right), \tag{3}$$

where $u(z)$ and $v(z)$ are the slowly varying amplitudes of the forward and backward propagating fields, respectively, and satisfy the coupled-mode equations

$$u'(z) = +i\left[\delta(z)\,u(z) + \kappa(z)\,v(z)\right], \tag{4a}$$
$$v'(z) = -i\left[\delta(z)\,v(z) + \kappa(z)\,u(z)\right], \tag{4b}$$

where

$$\delta(z) = \Delta + \frac{\pi}{\Lambda_0}\sigma(z) - \phi'(z), \tag{5a}$$
$$\kappa(z) = \frac{\pi}{\Lambda_0}h(z). \tag{5b}$$

The quantities $\delta(z)$ and $\kappa(z)$ represent the local detuning and local coupling strengths, respectively. Equation (5a) shows that variations in the background refractive index $\sigma(z)$ have the same effect as variations in the period $\phi'(z)$. The local Bragg condition becomes $\delta(z) = 0$.

The reflectivity of the grating is

$$r(\Delta) = \lim_{z\to-\infty}\frac{v(z)}{u(z)}e^{2i\Delta z}, \tag{6}$$

with the condition $v(z) \to 0$ as $z \to \infty$ imposed. If there is no grating for $z < 0$, then $r(\Delta) = v(0)/u(0)$.

Although it is possible to analyze the coupled-mode equations in the form given in Eqs. (4), it is advantageous to introduce the following transformations [9]:

$$\mathcal{E}(z) = u(z) + v(z), \tag{7a}$$
$$\mathcal{H}(z) = u(z) - v(z), \tag{7b}$$
$$\epsilon(z) = \delta(z) + \kappa(z), \tag{7c}$$
$$\mu(z) = \delta(z) - \kappa(z). \tag{7d}$$

The coupled-mode equations then become

$$\mathcal{E}'(z) = i\,\mu(z)\,\mathcal{H}(z), \tag{8a}$$
$$\mathcal{H}'(z) = i\,\epsilon(z)\,\mathcal{E}(z). \tag{8b}$$

These equations correspond to the propagation of an electromagnetic plane wave with unit frequency through a medium with dielectric permittivity $\epsilon(z)$ and magnetic permeability $\mu(z)$. The local refractive index in this effective medium satisfies

$$n_{\text{eff}}(z) = \sqrt{\epsilon(z)\mu(z)} = \sqrt{\delta^2(z) - \kappa^2(z)}. \tag{9}$$

This local effective index is real when $|\delta(z)| > \kappa(z)$ and the fields at this point in the grating are (locally) propagating waves, which correspond to wavelengths outside the local reflection band. This local effective index is pure imaginary when $|\delta(z)| < \kappa(z)$ and the fields at this point in the grating are (locally) evanescent waves, which correspond to wavelengths inside the local reflection band and any field is strongly reflected when it reaches this region of the grating.

III. REFLECTION-BAND DIAGRAMS

Information about the local photonic band gap or reflection band in a slowly varying grating can be conveniently displayed on a *reflection-band diagram.* Some examples are Figs. 1, 4, and 6. These diagrams are analyzed individually in Sec. V.

Each point on the diagram corresponds to a particular detuning Δ for the incident wave and a particular point z along the grating. The local Bragg condition $\delta(z) = 0$ is shown by a solid curve given by

$$\Delta = \phi'(z) - \frac{\pi}{\Lambda_0}\sigma(z). \tag{10a}$$

The shaded region surrounding the solid curve shows the extent of the local photonic band gap or reflection band. The band gap edges are given by the condition $\delta(z) = \pm\kappa(z)$ which yields the curves

$$\Delta = \phi'(z) - \frac{\pi}{\Lambda_0}\sigma(z) \pm \frac{\pi}{\Lambda_0}h(z). \tag{10b}$$

Thus, the width of the local photonic band gap is $2\pi h(z)/\Lambda_0$. If a point lies in a shaded region, then the fields in the grating at that point and for that value of the detuning are evanescent; if it lies in an unshaded region, the local fields are propagating.

The qualitative features of the reflectance spectrum of any slowly varying Bragg grating can be obtained directly from the band diagram. For each incident wavelength, a horizontal line drawn across the band diagram at the corresponding value of the detuning Δ gives the behavior of the fields in the grating. The incident wave travels freely through the unshaded regions, but is strongly reflected whenever it encounters a shaded region; a very small amount is transmitted through the evanescent region. This is analogous to the strong reflections in barrier tunneling problems in quantum mechanics. In addition to the strong reflections at the band edges, there are weak reflections at the front and back ends of the grating; this can be viewed essentially as an impedance mismatch effect.

Several examples of band diagrams are analyzed in Sec. V.

IV. PHASE-INTEGRAL METHOD (WKB)

Semianalytical approximations are obtained for the reflectance spectrum using the phase-integral or WKB method [10]. The field in each propagating or evanescent region is written as the product of the local oscillatory or exponentially varying field and a slowly varying amplitude. The WKB method is essentially a standard slowly varying amplitude analysis supplemented by a procedure to match the fields across the turning points between the propagating and evanescent regions.

There are three separate effects that are treated in the WKB analysis here. The first effect is barrier tunneling through evanescent regions (where the wave is within the local photonic band gap). The relation between the incident, reflected, and transmitted waves can be described by a 2×2 transfer matrix $\mathsf{W}(\theta)$ whose explicit form is given in the Appendix. The barrier factor θ is given by

$$\theta = \int |n_{\text{eff}}(z)| dz, \tag{11}$$

where the integration extends over the length of the barrier (or evanescent) region. The barrier factor θ can be regarded as a generalization of the grating strength κL associated with uniform gratings.

The second effect is simple propagation through regions of the grating where the wave is outside the local photonic gap and only weakly interacts with the grating. This is described by a transfer matrix $\mathsf{P}(\phi)$ where the phase factor ϕ is given by

$$\phi = \int n_{\text{eff}}(z) dz, \tag{12}$$

where the integration extends over the length of the propagating region.

The final effect is reflection at the ends of a finite grating which is described by a matrix $\Gamma(\mathcal{Z})$, where $\mathcal{Z}$ is the local impedance which satisfies

$$\mathcal{Z}^2 = \frac{\mu}{\epsilon} = \frac{\delta - \kappa}{\delta + \kappa}. \tag{13}$$

The choice of square root is detailed in the Appendix.

The total effect of the grating is then given by the product of the appropriate transfer matrices. The WKB derivation and the explicit form of all the various transfer matrices are given in the Appendix.

However, unlike the situation in quantum mechanics, there is a further complication here. The effective refractive index can be real in two different ways. First, if both ϵ and μ are positive, n_{eff} is real and waves propagate freely. Such a region will be labeled a "normal" propagating region. However, if both ϵ and μ are negative, n_{eff} is still real and waves propagate freely. Such a region will be labeled an "anomalous" propagating region. There is nothing to distinguish the propagation of waves in either region on their own, but when a normal and anomalous region are separated by an evanescent region the connection between the reflected and transmitted waves is different from the situation when an evanescent region separates two propagating regions of the same kind (i.e., both normal or both anomalous).

The WKB analysis possesses certain advantages over a direct solution of the coupled-mode equations. First, for some structures closed form expressions or accurate approximations to the phase integrals can be obtained. In such cases, the WKB result can be calculated much faster than the coupled-mode solution. Although computational speed is seldom an issue, such advantages may be important in the interactive design or optimization of nonuniform gratings. More importantly, however, the WKB results isolate and identify the features of the grating that are associated with the various features of the reflectance spectrum, giving a much deeper understanding of nonuniform gratings.

V. EXAMPLES

A. Linearly chirped grating

Linearly chirped gratings are of interest in dispersion compensation [6]. As will be shown below, different incident frequencies (detunings) can be delayed by different amounts; this effect can be used to compensate for any chromatic dispersion experienced after long distance propagation. Extremely accurate results for chirped gratings are obtained here, much faster than and without direct solution of the coupled-mode equations.

Consider a linearly chirped grating with a refractive index profile

$$n(z) = n_0 \left[1 + 2h_0 \cos\left(2\pi \frac{z}{\Lambda_0}(1 + Cz)\right)\right], \quad -\frac{L}{2} \le z \le \frac{L}{2}, \tag{14}$$

where C is a chirp parameter. The local detuning and coupling strengths are

$$\delta(z) = \Delta - \frac{2\pi C}{\Lambda_0} z, \tag{15a}$$

$$\kappa(z) = \kappa_0 = \frac{\pi h_0}{\Lambda_0}. \tag{15b}$$

The reflection-band diagram is shown in Fig. 1 and consists of a sloped line representing the Bragg condition surrounded by a photonic band gap of constant width. From Eqs. (10) the Bragg condition is

$$\Delta = 2\pi C z / \Lambda_0 \tag{16a}$$

and the edges of the photonic band gap are given by

$$\Delta = \pi(2Cz \pm h_0)/\Lambda_0 \tag{16b}$$

and, in this case, the reflection band has a constant height of $2\pi h_0/\Lambda_0$. For each detuning Δ in the range $|\Delta| < \pi(LC - h_0)/\Lambda_0$ the grating can be divided into three regions as shown in Fig. 1: a single evanescent region of length L_{eff} sandwiched between two propagating regions of length L_i and L_f, respectively. Outside this range of detunings, the interaction with the grating is

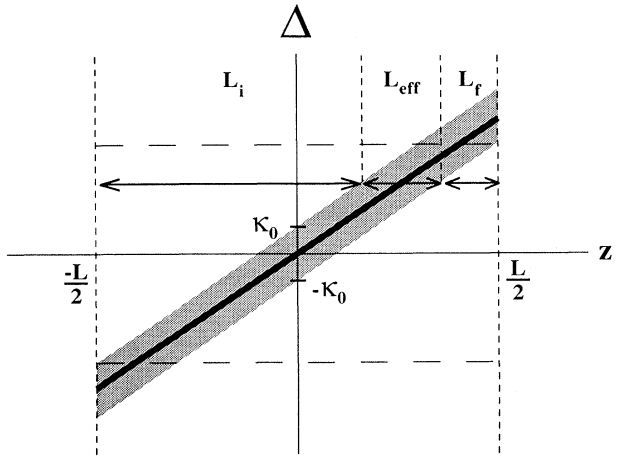

FIG. 1. Reflection-band diagram for a linearly chirped grating. The solid diagonal line represents the Bragg condition, and the shaded region the extent of the local photonic band gap. For any detuning, the grating divides into three regions: a central barrier of length L_{eff} surrounded by propagating regions of lengths L_i and L_f.

very weak and the reflectance spectrum is similar to that for a uniform grating outside its reflection band, and will not be considered further here.

The lengths of the regions shown in Fig. 1 can be calculated easily from Eqs. (16). In particular, the length of the evanescent region (where all the strong interaction occurs) is $L_{\text{eff}} = h_0/|C|$. Treating this interaction region as a *uniform* grating, the effective grating strength is approximately

$$\kappa_0 L_{\text{eff}} = \frac{\pi h_0^2}{|C|\Lambda_0}. \tag{17}$$

This estimate differs from the more accurate WKB result obtained later only by a numerical factor.

From Fig. 1 the distance traveled down the grating before encountering an evanescent region varies with detuning (or frequency). Consequently, upon reflection, waves with higher frequencies are delayed more than those with lower frequencies (or vice versa if the grating is reversed). The delay time is approximately $n_0 L_{\text{delay}}/c_0$, where c_0 is the speed of light *in vacuo* and

$$L_{\text{delay}} = 2L_i = \frac{\Lambda_0}{\pi C}\Delta + \left(L - \frac{h_0}{C}\right). \tag{18}$$

This simple estimate of the delay is compared in Fig. 2 with the exact delay calculated from the coupled-mode equations using

$$L_{\text{delay}} = \frac{\partial \varphi}{\partial \Delta}, \tag{19}$$

where φ is the phase of the reflectivity $r = |r|\exp(i\varphi)$. The slope of the simple estimate is slightly overestimated because the phase velocity c_0/n_{eff} over the section L_i is not constant but increases as the band gap is approached, resulting in a smaller delay. The simple estimate also does not predict the oscillations that arise from interference of waves reflected from the front and back of the gratings.

The WKB approximation for the reflectivity is obtained by multiplying together five 2×2 transfer matrices

$$\begin{bmatrix} u(0) \\ v(0) \end{bmatrix} = \Gamma(\mathcal{Z}_i)\cdot \mathsf{P}(\phi_i)\cdot \mathsf{W}(\theta)\cdot \mathsf{P}^{-1}(\phi_f)\cdot \Gamma^{-1}(\mathcal{Z}_f)\begin{bmatrix} u(L) \\ v(L) \end{bmatrix}. \tag{20}$$

The matrix W represents the effects of tunneling through and reflection from the evanescent region and the barrier factor is

$$\theta = \int_{z_1}^{z_2} |n_{\text{eff}}(z)|dz = \frac{\pi^2 h_0^2}{4|C|\Lambda_0}, \tag{21}$$

where z_1 and z_2 are the turning points at the ends of the evanescent region. Apart from a numerical factor of 4 the barrier factor θ agrees with the approximate expression for the effective grating strength in Eq. (17). The matrices P represent propagation over the regions of length L_i and L_f with accumulated phases

$$\phi_- = \int_{-\frac{L}{2}}^{z_1} n_{\text{eff}}(z)\,dz = \frac{\Lambda_0}{4\pi C}\left\{\delta\left(-\frac{L}{2}\right) n_{\text{eff}}\left(-\frac{L}{2}\right) - \frac{\pi^2 h_0^2}{\Lambda_0^2}\ln\left|\frac{\delta(-\frac{L}{2}) + n_{\text{eff}}(-\frac{L}{2})}{\pi h_0/\Lambda_0}\right|\right\}, \tag{22a}$$

$$\phi_+ = \int_{z_2}^{\frac{L}{2}} n_{\text{eff}}(z)\,dz = -\frac{\Lambda_0}{4\pi C}\left\{\delta\left(\frac{L}{2}\right) n_{\text{eff}}\left(\frac{L}{2}\right) - \frac{\pi^2 h_0^2}{\Lambda_0^2}\ln\left|\frac{\delta(\frac{L}{2}) + n_{\text{eff}}(\frac{L}{2})}{\pi h_0/\Lambda_0}\right|\right\}. \tag{22b}$$

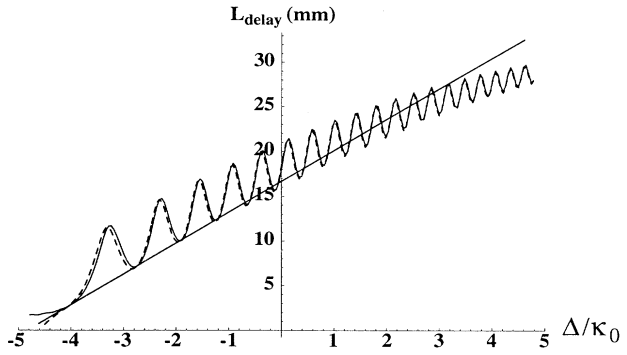

FIG. 2. Effective delay length on reflection from a linearly chirped grating vs normalized detuning Δ/κ_0. The straight line is a crude estimate of the chirp using the reflection-band diagram. The dashed curve is the WKB approximation. The solid curve is the coupled-mode analysis. The oscillations are due to interference of small reflections from the ends of the grating.

The matrices Γ represent the effects of reflection at the ends of the grating with impedances

$$\mathcal{Z}_i = \frac{\mu(-L/2)}{n_{\text{eff}}(-L/2)}, \tag{23a}$$

$$\mathcal{Z}_f = \frac{\mu(L/2)}{n_{\text{eff}}(L/2)}. \tag{23b}$$

All of the WKB quantities for a linearly chirped grating have been evaluated in closed form. The reflectivity can be obtained by evaluating the above explicit expressions and multiplying together the transfer matrices; this is much faster than solving the pair of coupled differential equations. The numerical and WKB results for the reflectance $|r|^2$ are compared in Fig. 3. The accuracy obtained for the phase of the reflectivity is demonstrated in Fig. 2. The grating analyzed has an index modulation of $h_0 = 10^{-4}$, a period of $\Lambda_0 = 0.5$ μm, a length of $L = 2$ cm, and a chirp of $C = 3 \times 10^{-5}$ mm^{-1}, which gives a grating with an average reflectance of 96% over the central range of detunings. Except at the edges of this region the agreement between the exact and WKB results is excellent. This agreement improves for stronger gratings. For weaker gratings the errors are slightly larger: for a grating where the maximum reflectance is only 85% the error in the WKB result is only about 3%, and the agreement in the phase remains as good as in Fig. 2.

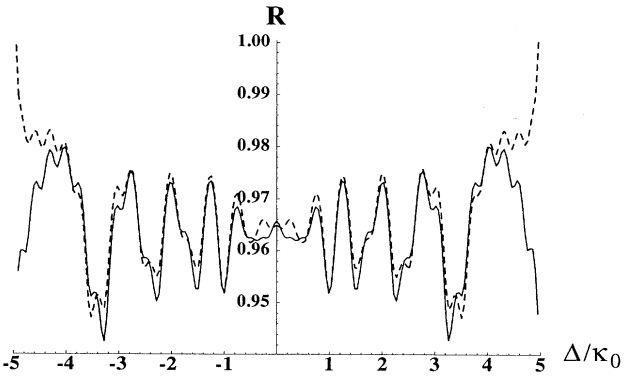

FIG. 3. Reflection spectrum for a linearly chirped grating with $h_0 = 10^{-4}$, $\Lambda_0 = 0.5$ μm, $L = 20$ mm, and $C = 3 \times 10^{-5}$ mm^{-1}. The dashed curve is the WKB approximation. The solid curve is the coupled-mode analysis.

B. Moiré gratings

Moiré gratings are of interest for fiber grating resonators and very narrow band filter responses [4]. A moiré grating can be considered as the superposition of two uniform gratings with slightly different periods. The refractive index profile has a typical interference beat pattern. Consider a moiré grating which is exactly two beat lengths long with a profile

$$n(z) = n_0 \left[1 + 2h_0 \sin\left(2\pi\frac{z}{L}\right) \cos\left(2\pi\frac{z}{\Lambda_0}\right)\right]. \tag{24}$$

In contrast to the chirped grating, here, the detuning is constant $\delta(z) = \Delta$ and the local coupling strength varies sinusoidally

$$\kappa(z) = \kappa_0 \sin\left(2\pi\frac{z}{L}\right), \tag{25}$$

where $\kappa_0 = \pi h_0/\Lambda_0$. Thus, the width of the local photonic band gap also varies sinusoidally. The reflection-band diagram for this moiré grating is shown in Fig. 4.

The first and second halves of the grating are identical except that the grating strength over the second half of the grating as given by Eq. (25) is negative. From Eq. (1),

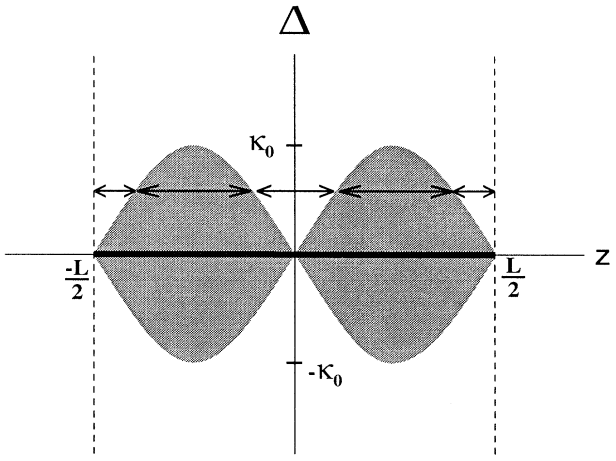

FIG. 4. Reflection-band diagram for a moiré grating. The solid line represents the Bragg condition and the shaded region the extent of the local photonic band gap. The vertical dashed line represent a π phase change in the center of the grating. The horizontal dashed line shows the length of a resonant cavity bounded by two barrier regions.

this is equivalent to having a positive grating strength but having a phase shift of $2\phi(z) = \pi$ over the second half of the grating. The discontinuous phase jump between the two halves of the grating is also indicated by the crossing over of the two photonic band edges in the center of the reflection-band diagram.

For any detuning in detuning range $|\Delta| < \kappa_0$ the grating divides into five sections: a central propagating region (or cavity) surrounded by two evanescent regions (or barriers) and finally an initial and a final propagating section. The central cavity region behaves exactly like a Fabry-Pérot resonator and the reflectance spectrum of the grating should show transmission fringes whenever the phase change across the cavity (including the phase jump at the center) gives rise to destructive interference of the waves reflected from each end of the cavity. This cavity condition is

$$2\phi_c = 2\int_{-z_1}^{z_1} n_{\text{eff}}(z)dz = n\pi, \tag{26a}$$

where

$$z_1 = \frac{L}{2\pi}\sin^{-1}\left(\frac{\Delta}{\kappa_0}\right). \tag{26b}$$

For strong Moiré gratings the transmission fringes are extremely narrow and difficult to locate directly using a numerical solution. In fact, the WKB result was used to obtain an initial estimate of the location of the fringes, which was then improved numerically. The exact reflectance spectrum for a moiré grating with index modulation of $h_0 = 2 \times 10^{-4}$, a period of $\Lambda_0 = 0.5$ μm, and a length of $L = 3$ cm is shown in Fig. 5 and a comparison of the exact and WKB results for the transmission resonances is given in Table I. In every case shown the error is less than 1% and in many cases much smaller still. The accuracy improves with grating strength, although this becomes harder to verify directly, as the couple-mode analysis itself becomes less accurate.

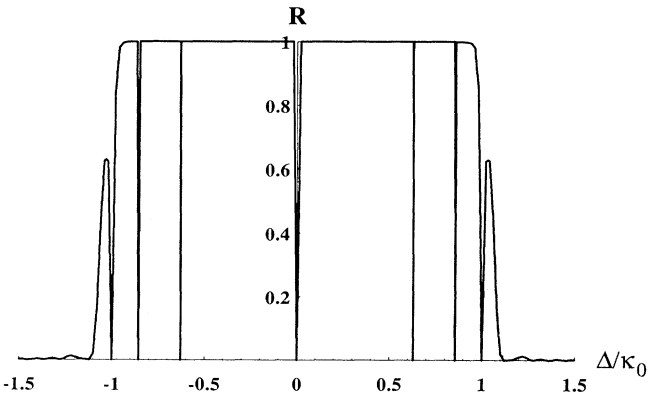

FIG. 5. Reflection spectrum for a moiré grating with $h_0 = 2 \times 10^{-4}$, $\Lambda_0 = 0.5$ μm, $L = 30$ mm. The transmission fringes are the result of interference effects in the resonant cavities seen in the band diagram. A comparison with the WKB predictions for the fringe locations is given in Table I.

TABLE I. Comparison of WKB approximation and exact coupled-mode (CM) calculation of the location of transmission fringes in the reflectance spectrum of a moiré grating. The location of the fringes is given by the normalized detuning Δ/κ_0.

$(\kappa_0 L, n)$	WKB [Eqs. (26)]	CM
(10,1)	0.9971	1.0050
(20,1)	0.7577	0.7544
(20,2)	0.9971	0.9982
(30,1)	0.6290	0.6282
(30,2)	0.8585	0.8559
(30,3)	0.9971	0.9969
(60,1)	0.4514	0.4513
(60,2)	0.6290	0.6288
(60,3)	0.7577	0.7573
(60,4)	0.8585	0.8579
(60,5)	0.9384	0.9370
(60,6)	0.9971	0.9963

The WKB transfer matrix for the moiré grating is

$$\Gamma(\mathcal{Z}_i)\cdot \mathsf{P}(\tfrac{1}{2}\phi_c)\cdot \mathsf{W}(\theta)\cdot \mathsf{P}(\phi_c)\cdot \mathsf{W}(\theta)\cdot \mathsf{P}^{-1}(\tfrac{1}{2}\phi_c)\cdot \Gamma^{-1}(\mathcal{Z}_f), \tag{27}$$

where ϕ_c is given above, the barrier factor θ is

$$\theta = \int_{z_1}^{L-z_1} |n_{\text{eff}}(z)|dz \tag{28}$$

and

$$\mathcal{Z}_i = \mathcal{Z}_f = \text{sgn}(\Delta). \tag{29}$$

The phase integrals for ϕ_c and θ can be evaluated in terms of hypergeometric functions. The simple power law approximations to these hypergeometric functions given below are also useful and reasonably accurate expressions:

$$\phi_c = \frac{\Delta^2 L}{8\kappa_0}\,{}_2F_1\left(\frac{1}{2},\frac{1}{2},2;\frac{\Delta^2}{\kappa_0^2}\right) \approx \frac{\kappa_0 L}{2\pi}\left|\frac{\Delta}{\kappa_0}\right|^{9/4}, \tag{30a}$$

$$\theta = \left(\frac{\kappa_0 L}{4} - \frac{\Delta^2 L}{4\kappa_0}\right)\,{}_2F_1\left(\frac{1}{2},\frac{1}{2},2;1-\frac{\Delta^2}{\kappa_0^2}\right) \approx \frac{\kappa_0 L}{\pi}\left(1-\left|\frac{\Delta}{\kappa_0}\right|^{7/4}\right). \tag{30b}$$

Despite their complexity, evaluating the above exact expressions is significantly more efficient than solving coupled differential equations.

C. Gaussian-tapered gratings

Gratings written holographically into fibers or waveguides have a refractive index profile which is determined by the intensity profile of the writing beams. If the index

change is taken to be proportional to the intensity of the writing beam, then a grating produced by two interfering identical beams has a refractive index profile that can be written in the form

$$n(z) = n_0 \left[1 + 4h_0 f(z) \cos^2\left(\pi \frac{z}{\Lambda_0}\right)\right] \tag{31a}$$

$$= n_0 \left[\{1 + 2h_0 f(z)\} + 2h_0 f(z) \cos\left(2\pi \frac{z}{\Lambda_0}\right)\right], \tag{31b}$$

where $f(z)$ is the profile of the interfering beams. Note that both the coefficient of the oscillatory part and the average refractive index vary according to the beam profile. Thus, even though the grating period Λ_0 is a constant, the local Bragg wavelength varies along the grating because of the slowly varying average refractive index. The local detuning and coupling strength are

$$\delta(z) = \Delta + 2\kappa_0 f(z), \tag{32a}$$

$$\kappa(z) = \kappa_0 f(z), \tag{32b}$$

where $\kappa_0 = \pi h_0/\Lambda_0$. The second term in $\delta(z)$ is the *self-induced chirp* that arises from the varying average refractive index.

An important example is when the writing beams have a Gaussian profile with $f(z) = \exp(-z^2/w^2)$ where we also assume for convenience that the exponential tails of the grating extend to infinity. This structure has been briefly treated in an earlier paper [9].

The reflection-band diagram for the Gaussian grating is shown in Fig. 6. The Bragg condition is represented by the line

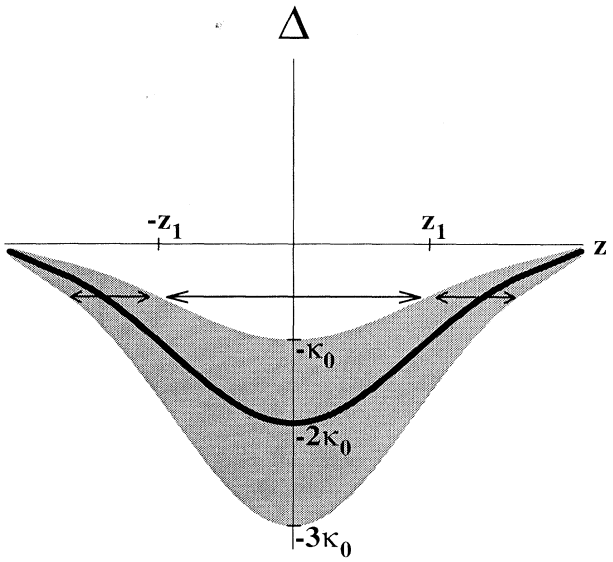

FIG. 6. Reflection-band diagram for a Gaussian grating. The solid curve represents the Bragg condition and the shaded region the extent of the local photonic band gap. The horizontal dashed line shows the length of a resonant cavity bounded by two barrier regions. The barrier regions are produced by the tails of the Gaussian beam and are weak.

$$\Delta = -2\kappa_0 \exp(-z^2/w^2). \tag{33}$$

The width of the local photonic band gap is $2\kappa_0 \exp(-z^2/w^2)$.

From the band diagram we see that for detunings in the range $-\kappa_0 < \Delta < 0$ there is a Fabry-Pérot type cavity similar to that in the moiré grating. The cavity condition here is

$$2\phi_c = 2\int_{-z_1}^{z_1} n_{\text{eff}}(z)dz = (2n+1)\pi, \tag{34a}$$

where

$$z_1 = w\sqrt{\ln\left|\frac{\kappa_0}{\Delta}\right|}. \tag{34b}$$

The reflectance spectrum for a Gaussian grating with $\kappa_0 = \pi h_0/\Lambda_0 = 1\ \text{mm}^{-1}$ and $w = 30$ mm is shown in Fig. 7. Transmission fringes occur as expected only in the region $-\kappa_0 < \Delta < 0$. The reflectance is virtually one over the range $-3\kappa_0 < \Delta < -\kappa_0$ where the band diagram has a single strong barrier, and the reflectance drops to virtually zero outside these ranges. The region with the transmission fringes is analyzed in detail.

A comparison of the location of the transmission fringes using this cavity condition (which corresponds to a first-order WKB calculation) and using coupled-mode analysis is given in Table II. The agreement improves as the strength of the grating increases. The agreement is also better for fringes deeper within the reflection band (Δ close to $-\pi h_0/\Lambda_0$). However, the performance of the WKB approximation is not as impressive as for the chirped and moiré gratings. The reason can be seen in Fig. 6. The resonant cavity near the edge of the reflection band (for Δ close to zero) is bounded by two very narrow barrier regions produced by the tails of the Gaussian beam profile. WKB analysis does not work as well for weak barriers. A *second-order* WKB expression for the cavity phase ϕ_c is given in Eq. (A13) and the corresponding results are tabulated in Table II. The second-order results are, in general, closer to the exact coupled-mode analysis.

The WKB transfer matrix for the Gaussian grating is

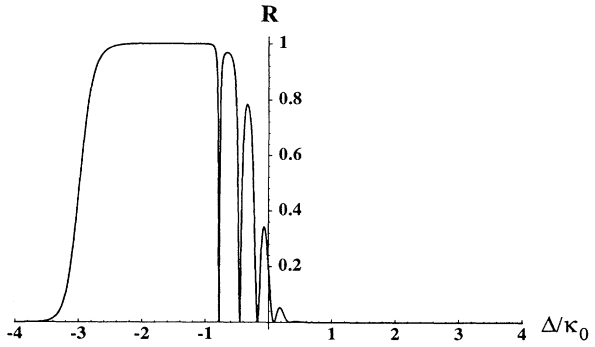

FIG. 7. Reflection spectrum for a Gaussian grating with $\kappa_0 = \pi h_0/\Lambda_0 = 1\ \text{mm}^{-1}$ and $L = 30$ mm. Transmission fringes occur over the region $-\kappa_0 < \Delta < 0$.

TABLE II. Comparison of both first- and second-order WKB approximations and exact CM calculation of the location of transmission fringes in the reflectance spectrum of a Gaussian-tapered grating. The location of the fringes is given by the normalized detuning Δ/κ_0.

$(\kappa_0 w, n)$	WKB [Eqs. (34)]	WKB2 [Eq. (A13)]	CM
(10,1)	-0.5033	-0.4425	-0.2239
(20,1)	-0.7356	-0.6910	-0.6549
(20,2)	-0.2994	-0.2716	-0.1873
(30,1)	-0.8198	-0.7862	-0.7822
(30,2)	-0.5033	-0.4764	-0.4537
(30,3)	-0.2376	-0.2193	-0.1721
(60,1)	-0.9079	-0.8888	-0.8996
(60,2)	-0.7356	-0.7172	-0.7245
(60,3)	-0.5775	-0.5611	-0.5633
(60,4)	-0.4323	-0.4180	-0.4147
(60,5)	-0.2994	-0.2874	-0.2782
(60,6)	-0.1790	-0.1695	-0.1533

$$\Gamma(\mathcal{Z}_i)\cdot \mathsf{P}(\phi_i)\cdot \mathsf{W}(\theta)\cdot \mathsf{P}(\phi_c)\cdot \mathsf{W}(\theta)\cdot \mathsf{P}^{-1}(\phi_f)\cdot \Gamma^{-1}(\mathcal{Z}_f), \tag{35}$$

where $\mathcal{Z}_i = \mathcal{Z}_f = \mathrm{sgn}(\Delta)$, and the barrier and phase integrals are defined as before. Unlike the previous cases, the phase integrals for ϕ_c and θ cannot be evaluated in closed form; however, simple power law approximations to these integrals are

$$\phi_c = \sqrt{3\pi}\kappa_0 w\left(1+\frac{\Delta}{\kappa_0}\right)^{5/4}, \tag{36a}$$

$$\theta = 0.416\,536\kappa_0 w\left(\frac{\Delta}{\kappa_0}\right)^{2}. \tag{36b}$$

The coupled-mode and (first-order) WKB results for the reflectance spectrum of a Gaussian grating with $\kappa_0 = \pi h_0/\Lambda_0 = 2\ \mathrm{mm}^{-1}$ and $w = 30$ mm are compared in Fig. 8. A comparison with the second-order WKB results for the same structure is shown in Fig. 9. The strength

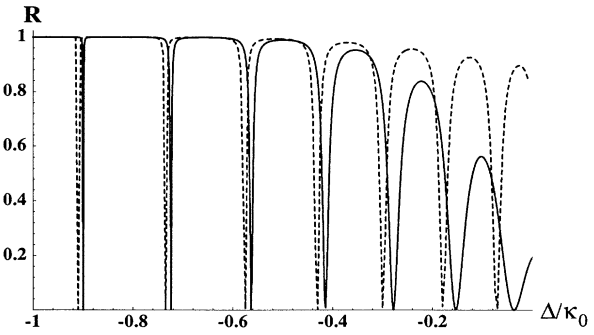

FIG. 8. Reflection spectrum for a Gaussian grating with $\kappa_0 = \pi h_0/\Lambda_0 = 2\ \mathrm{mm}^{-1}$ and $L = 30$ mm. The dashed curve is the first-order WKB approximation. The solid curve is the coupled-mode analysis. The agreement is better near the center of the reflection band.

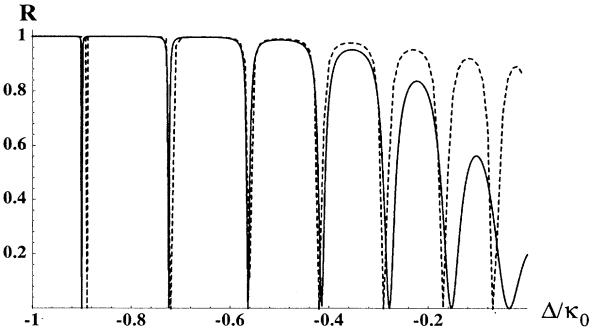

FIG. 9. Second-order WKB results for the same structure as in Fig. 8.

of the reflectance for detunings close to the edge of the reflection band is overestimated by the WKB approximations for reasons similar to those discussed above: the weakness of the barrier regions produced by the tails of the Gaussian beam profile.

VI. CONCLUSION

Reflection-band diagrams provide a succinct and extremely useful tool in understanding the properties of nonuniform gratings. The locations and extents of the local photonic band gaps within the gratings provide information about the strength and phase of the reflection coefficient. The qualitative information provided by the reflection-band diagrams can be supplemented by a WKB analysis of the grating, and the propagating or evanescent fields within the grating. For some structures, the WKB analysis provides accurate analytical approximations for the reflectivities, which obviates the need to numerically solve coupled-mode equations. In other cases, the WKB phase integrals must be evaluated numerically, or approximated by other functions. However, this can still be more computationally efficient than repeatedly solving the coupled-mode equations.

The most important feature of the combined band diagram and WKB approach is that it identifies the regions and features of the grating that are responsible for the observed reflectance characteristics, and it is this information that will be of benefit in the analysis and design of nonuniform gratings for specific applications.

ACKNOWLEDGMENTS

The author acknowledges useful discussions with C. M. de Sterke and J. E. Sipe. The author also thanks the Australian Research Council for providing financial support. The Optical Fibre Technology Centre is a partner in the Australian Photonics Cooperative Research Centre.

APPENDIX: WKB ANALYSIS

Different regions have to be considered in the WKB analysis depending upon the signs of $\epsilon(z)$ and $\mu(z)$. The local effective index $n_{\text{eff}}(z)$ is defined by

$$n_{\text{eff}}(z) = \begin{cases} \sqrt{\epsilon(z)\mu(z)}, & \epsilon(z)\mu(z) > 0 \\ i\sqrt{-\epsilon(z)\mu(z)}, & \epsilon(z)\mu(z) < 0. \end{cases} \tag{A1}$$

The local impedance $\mathcal{Z}(z)$ is defined by

$$\mathcal{Z}(z) = \begin{cases} \sqrt{\mu(z)/\epsilon(z)}, & \mu(z) > 0 \;\; \epsilon(z) > 0 \\ -\sqrt{\mu(z)/\epsilon(z)}, & \mu(z) < 0 \;\; \epsilon(z) < 0 \\ i\sqrt{-\mu(z)/\epsilon(z)}, & \mu(z) > 0 \;\; \epsilon(z) < 0 \\ -i\sqrt{-\mu(z)/\epsilon(z)}, & \mu(z) < 0 \;\; \epsilon(z) > 0. \end{cases} \tag{A2}$$

The first-order WKB or slowly varying amplitude solutions for the effective fields $\mathcal{E}$ and $\mathcal{H}$ satisfying the effective-medium relations in Eqs. (8) are then given by

$$\mathcal{E}(z) = \sqrt{|\mathcal{Z}(z)|}\left\{A\exp\left[+i\int_a^z n_{\text{eff}}(z)\,dz\right] + B\exp\left[-i\int_a^z n_{\text{eff}}(z)\,dz\right]\right\}, \tag{A3a}$$

$$\mathcal{H}(z) = \frac{\sqrt{|\mathcal{Z}(z)|}}{\mathcal{Z}(z)}\left\{A\exp\left[+i\int_a^z n_{\text{eff}}(z)\,dz\right] - B\exp\left[-i\int_a^z n_{\text{eff}}(z)\,dz\right]\right\}. \tag{A3b}$$

The lower range of integration in the phase can be chosen for convenience, and is chosen here to be the turning point.

The original coupled-mode amplitudes u and v can be represented in terms of the above WKB solutions by the following convenient matrix relation:

$$\begin{bmatrix} u(z) \\ v(z) \end{bmatrix} = \Gamma(\mathcal{Z}) \cdot \mathsf{P}(\phi) \begin{bmatrix} A \\ B \end{bmatrix}, \tag{A4}$$

where

$$\phi = \int_a^z n_{\text{eff}}(z)\,dz. \tag{A5}$$

The propagation matrix is

$$\mathsf{P}(\phi) = \begin{bmatrix} e^{i\phi} & 0 \\ 0 & e^{-i\phi} \end{bmatrix}. \tag{A6}$$

The impedance matrix is

$$\Gamma(\mathcal{Z}) = \frac{\sqrt{|\mathcal{Z}|}}{2\mathcal{Z}} \begin{bmatrix} \mathcal{Z}+1 & \mathcal{Z}-1 \\ \mathcal{Z}-1 & \mathcal{Z}+1 \end{bmatrix}. \tag{A7}$$

The WKB solutions in Eqs. (A3) lose their validity at points z where $n_{\text{eff}}(z) = 0$. The WKB solutions on either side of such turning points must be connected using the WKB connection formulas. If A_+ and B_+ represent the solution in the region where $n_{\text{eff}}^2(z) > 0$ and A_- and B_- represent the solution in the region where $n_{\text{eff}}^2(z) < 0$, then there are two connection formulas:

$$\begin{bmatrix} A_+ \\ B_+ \end{bmatrix} = \frac{\sqrt{2}}{8} \begin{bmatrix} 1-i & 1+i \\ 1+i & 1-i \end{bmatrix} \begin{bmatrix} 3-\eta & 0 \\ 0 & 3+\eta \end{bmatrix} \begin{bmatrix} A_- \\ B_- \end{bmatrix}, \qquad \mu(z) = 0, \tag{A8a}$$

$$\begin{bmatrix} A_+ \\ B_+ \end{bmatrix} = \frac{\sqrt{2}}{8} \begin{bmatrix} 1+i & 1-i \\ 1-i & 1+i \end{bmatrix} \begin{bmatrix} 3-\eta & 0 \\ 0 & 3+\eta \end{bmatrix} \begin{bmatrix} A_- \\ B_- \end{bmatrix}, \qquad \epsilon(z) = 0, \tag{A8b}$$

where $\eta = \text{sgn}(\partial n_{\text{eff}}^2/\partial z)$.

Consider a barrier located at $a < z < b$. The coefficients describing the propagating solutions on either side of the barrier are related by the following connection formula:

$$\begin{bmatrix} A \\ B \end{bmatrix}_{z<a} = \mathsf{P}(\chi) \cdot \mathsf{W}(\theta) \cdot \mathsf{P}(\chi) \begin{bmatrix} A \\ B \end{bmatrix}_{z>b}, \tag{A9}$$

where

$$\theta = \int_a^b |n_{\text{eff}}(z)|\,dz \tag{A10}$$

is the barrier factor. The magnitude of the phase shift χ which occurs in the propagation matrix $\mathsf{P}(\chi)$ cannot be determined within the WKB approximation because of the one-sided nature of the connection formulas [10,11]; however, $\chi \to 0$ as the barrier becomes stronger. All results given here assume $\chi = 0$. Physically, the phase shift χ can be explained in terms of a slight penetration of the incident field into the barrier before reflection and is completely analogous to the well-known Goos-Hanchen effect at the core-cladding boundary in waveguides.

The form of the connection matrix depends on the nature of the two turning points:

$$\mathsf{W}(\theta) = \begin{bmatrix} (e^{\theta}+e^{-\theta}/4) & i(e^{\theta}-e^{-\theta}/4) \\ -i(e^{\theta}-e^{-\theta}/4) & (e^{\theta}+e^{-\theta}/4) \end{bmatrix}, \qquad \epsilon(a) = \epsilon(b) = 0, \tag{A11a}$$

$$\mathsf{W}(\theta) = \begin{bmatrix} (e^{\theta}+e^{-\theta}/4) & -i(e^{\theta}-e^{-\theta}/4) \\ i(e^{\theta}-e^{-\theta}/4) & (e^{\theta}+e^{-\theta}/4) \end{bmatrix}, \qquad \mu(a) = \mu(b) = 0, \tag{A11b}$$

$$\mathsf{W}(\theta) = \begin{bmatrix} i(e^{\theta} - e^{-\theta}/4) & (e^{\theta} + e^{-\theta}/4) \\ (e^{\theta} + e^{-\theta}/4) & -i(e^{\theta} - e^{-\theta}/4) \end{bmatrix},$$

$$\epsilon(a) = \mu(b) = 0, \quad \text{(A11c)}$$

$$\mathsf{W}(\theta) = \begin{bmatrix} -i(e^{\theta} - e^{-\theta}/4) & (e^{\theta} + e^{-\theta}/4) \\ (e^{\theta} + e^{-\theta}/4) & i(e^{\theta} - e^{-\theta}/4) \end{bmatrix},$$

$$\mu(a) = \epsilon(b) = 0. \quad \text{(A11d)}$$

The above results and transfer matrices can be combined to give the transfer matrix for any structure. The reflection and transmission coefficients are then obtained from the elements of the resultant transfer matrix

$$\begin{bmatrix} u(0) \\ v(0) \end{bmatrix} = \begin{bmatrix} 1/t & r^*/t^* \\ r/t & 1/t^* \end{bmatrix} \begin{bmatrix} u(L) \\ v(L) \end{bmatrix}. \quad \text{(A12)}$$

Finally, the WKB analysis here is a first-order analysis. The results can be extended to second order. This will not be done here, except for a single result. The phase on propagation to second order is given by

$$\phi = \int n_{\text{eff}}(z)\, dz - \int \frac{[\mathcal{Z}'(z)]^2}{8n_{\text{eff}}(z)[\mathcal{Z}(z)]^2}\, dz. \quad \text{(A13)}$$

A simple physical interpretation of the second integral is not known at this stage.

As a rough estimate, the first-order WKB approximations are expected to be valid when the following slowly varying condition is satisfied:

$$[\mathcal{Z}'(z)]^2 \ll 8n_{\text{eff}}^2(z)[\mathcal{Z}(z)]^2. \quad \text{(A14)}$$

In practice, the WKB approximations can be accurate beyond the limits given by the above inequality.

[1] K. O. Hill, Appl. Opt. **13**, 1853 (1974).
[2] H. Kogelnik, in *Integrated Optics*, edited by T. Tamir (Springer-Verlag, Berlin, 1975), pp. 15–81.
[3] C. Elachi, Proc. IEEE **64**, 1666 (1976).
[4] C. M. Ragdale, D. Reid, and I. Bennion, Proc. Soc. Photo-Opt. Instrum. Eng. **1171**, 148 (1989).
[5] G. I. Stegeman and D. G. Hall, J. Opt. Soc. Am. A **7**, 1387 (1990).
[6] F. Ouellette, Opt. Lett. **12**, 847 (1987).
[7] D. Reid *et al.*, Electron. Lett. **26**, 10 (1990).
[8] R. Kashap *et al.*, BT Technol. J **11**, (1993).
[9] J. Sipe, L. Poladian, and C. M. de Sterke, J. Opt. Soc. Am. A (to be published).
[10] Bender and Orsag, *Advanced Mathemetical Methods for Scientists and Engineers* (McGraw-Hill, New York, 1978).
[11] N. Froman and P. O. Froman, *JWKB Approximation* (North-Holland, Amsterdam, 1965).